*Geophys. J. Int.* (2000) **142,** 000–000

# An Arbitrary High Order Discontinuous Galerkin Method for Elastic Waves on Unstructured Meshes II: Discretization of External Source Terms

Michael Dumbser[1],Martin Käser[1]

[1] *Department of Civil and Environmental Engineering, University of Trento, Trento, Italy*

**SUMMARY**

In this article we present a Discontinuous Galerkin scheme of arbitrary accuracy in space and time (ADER-DG scheme) to solve linear hyperbolic systems on unstructured triangular meshes in the presence of externally given source terms that may depend on space and time. The consideration of source terms is new since in previous articles on ADER-DG schemes only the homogeneous case was treated. We combine a Discontinuous Galerkin Method for space discretization with the ideas of the ADER (arbitrary high order derivatives) time integration approach. The time integration is performed via the so-called Cauchy-Kovalewski procedure using repeatedly the governing partial differential equation (PDE) itself. Thus we are able to construct a numerical method that is of arbitrary order of accuracy in space and time using only one single explicit step to integrate the PDE from one time level to another.

Two different cases of source terms are considered: continuous sources in space and time and point sources that are characterized by a Delta distribution in space and some continuous source time function. We emphasize that the presented method is able to deal with point sources at *any* position in the computational domain that does not necessarily need to coincide with a grid point. Interpolation is automatically performed by evaluation of the test functions at the source locations. The convergence studies for continuous sources in space and time demonstrate that also in the presence of source terms the scheme maintains very high order of accuracy uniformly in space and time. Applications of the proposed method to two classical benchmark problems of computational seismology involving point sources, namely Lamb's problem and Garvin's problem, and comparisons with the analytical solutions confirm the accuracy of the method as well as the correct treatment of free-surface boundary conditions.

**Key words:** elastic waves, discontinuous Galerkin method, arbitrary high order, unstructured meshes, source terms, Lamb's problem, Garvin's problem

## 1 INTRODUCTION

We present a new Discontinuous Galerkin (DG) finite element scheme for two space dimensions that uses the Arbitrary high order DERivatives (ADER) approach in order to solve linear hyperbolic systems with very high accuracy in both space *and* time on unstructured grids in the presence of externally given space-time dependent source terms. The ADER approach was first developed in a Finite Volume framework for linear and nonlinear hyperbolic systems, see e.g. (Toro 2001; Toro & Titarev 2002; Titarev & Toro 2002; Schwartzkopff, Dumbser & Munz 2002; Käser & Iske 2005).

The proposed numerical method is a straight-forward extension of the ADER-DG scheme presented in (Dumbser 2005; Dumbser & Munz 2005; Käser & Dumbser 2005) for the homogeneous case but this time also taking into account the source terms, both, in space and time discretization. The resulting ADER-DG scheme is again theoretically arbitrarily accurate in space and time, where temporal accuracy automatically matches the spatial accuracy.

The paper is structured as follows. In Section 2 we introduce the system of the elastic wave equations in the non-conservative velocity-stress formulation with source terms. The proposed DG scheme is presented in Section 3 together with the ADER approach where attention is mainly paid to the discretization of the externally given source term such that globally arbitrary accuracy in space and time can be maintained. For a more exhaustive presentation of the ADER-DG approach for the homogeneous case see (Käser & Dumbser 2005).

In Section 4 we investigate numerically the convergence rates of the scheme on the example of a fourth and sixth order ADER-DG scheme with an analytically given source term that is constructed such that the exact solution of the governing PDE is known. In Section 5 we show the application of the method for two classical test problems where non-trivial analytical solutions exist, namely Lamb's problem and Garvin's problem. For both test problems, unstructured meshes are very useful since they allow an easy refinement of the mesh close to the surface in order to capture well the surface waves.

## 2 ELASTIC WAVE EQUATIONS

The propagation of waves in an elastic medium is based on the theory of linear elasticity (Aki & Richards 2002; Bedford & Drumheller 1994). Combining the definition of strain caused by deformations (Hooke's law) and the equations of the dynamic relationship between acceleration and stress, the elastic wave equations can be derived as shown in (LeVeque 2002). Considering the two-dimensional elastic wave equation for an isotropic medium in velocity-stress formulation and admitting external sources (e.g. moments or body forces) leads to a linear hyperbolic system of the form

$$\begin{aligned}
\tfrac{\partial}{\partial t}\sigma_{xx} - (\lambda+2\mu)\tfrac{\partial}{\partial x}v - \lambda\tfrac{\partial}{\partial y}w &= S_1(x,y,t)\,, \\
\tfrac{\partial}{\partial t}\sigma_{yy} - \lambda\tfrac{\partial}{\partial x}v - (\lambda+2\mu)\tfrac{\partial}{\partial y}w &= S_2(x,y,t)\,, \\
\tfrac{\partial}{\partial t}\sigma_{xy} - \mu(\tfrac{\partial}{\partial x}w + \tfrac{\partial}{\partial y}v) &= S_3(x,y,t)\,, \\
\rho\tfrac{\partial}{\partial t}v - \tfrac{\partial}{\partial x}\sigma_{xx} - \tfrac{\partial}{\partial y}\sigma_{xy} &= \rho S_4(x,y,t)\,, \\
\rho\tfrac{\partial}{\partial t}w - \tfrac{\partial}{\partial x}\sigma_{xy} - \tfrac{\partial}{\partial y}\sigma_{yy} &= \rho S_5(x,y,t)\,,
\end{aligned} \tag{1}$$

where $\lambda$ and $\mu$ are the *Lamé constants* and $\rho$ is the mass density of the material. The normal stress components are given by $\sigma_{xx}$ and $\sigma_{yy}$, and the shear stress is $\sigma_{xy}$. The components of the particle velocities in $x$- and $y$-direction are denoted by $v$ and $w$, respectively.

The stresses and velocities are always assumed to be functions of time and space. The physical properties of the material are functions of space but are constant in time, i.e. $\lambda = \lambda(\vec{x})$, $\mu = \mu(\vec{x})$, and $\rho = \rho(\vec{x})$, with $\vec{x} = (x, y)$, in order to describe heterogeneous material.

For the sake of generality, we use the more compact form

$$\frac{\partial u_p}{\partial t} + A_{pq}\frac{\partial u_q}{\partial x} + B_{pq}\frac{\partial u_q}{\partial y} = S_p(x,y,t), \tag{2}$$

where $u_p$ is the vector of state, i.e. in the case of the elastic wave equations $u_p = (\sigma_{xx}, \sigma_{yy}, \sigma_{xy}, v, w)^T$ and $S_p(x,y,t)$ is the vector of space-time dependent source terms as given in (1). Here, we use classical tensor notation which implies summation over each index appearing twice. The matrices $A_{pq} = A_{pq}(\vec{x})$ and $B_{pq} = B_{pq}(\vec{x})$ are the space dependent Jacobian matrices as given in (Käser & Dumbser 2005).

## 3 DISCRETIZATION OF SOURCE TERMS WITHIN ADER-DG SCHEMES

For the details of the construction of the numerical scheme for the wave propagation operator on the left hand side of (2) we refer to (Käser & Dumbser 2005). In this article we focus on the discretization of the source terms on the right hand side of (2). In the presence of space-time dependent source terms we need to carefully incorporate them into the ADER Discontinuous Galerkin framework in order to maintain globally arbitrary accuracy in space and time.

As in (Käser & Dumbser 2005) the computational domain $\Omega \in \mathbb{R}^2$ is divided in conforming triangular elements $\mathcal{T}^{(m)}$ being addressed by a unique index $(m)$ and the numerical solution of (2) is represented as

$$\left(u_h^{(m)}\right)_p(\xi,\eta,t) = \hat{u}_{pl}^{(m)}(t)\Phi_l(\xi,\eta). \tag{3}$$

Furthermore, we suppose the matrices $A_{pq}$ and $B_{pq}$ to be locally constant inside an element $\mathcal{T}^{(m)}$.

### 3.1 Space-Time Continuous Source Terms

In order to perform high order time-discretization of the scheme we proceed as in the homogeneous case (Käser and Dumbser, 2005), replacing time-derivatives by space-derivatives using the governing PDE. However, the Cauchy-Kovalewski procedure gets more complicated if source terms are present. The original PDE (2) rewritten in $\xi\eta$-coordinates of the reference element results in

$$\frac{\partial u_p}{\partial t} + A^*_{pq}\frac{\partial u_q}{\partial \xi} + B^*_{pq}\frac{\partial u_q}{\partial \eta} = S_p. \tag{4}$$

The $k$-th time derivative as a function of pure space derivatives in the $\xi\eta$-reference system is the result of the Cauchy-Kovalewski procedure applied to (4) and is given by

$$\frac{\partial^k}{\partial t^k}u_p = (-1)^k\left(A^*_{pq}\frac{\partial}{\partial \xi} + B^*_{pq}\frac{\partial}{\partial \eta}\right)^k u_q + \sum_{s=0}^{k-1}(-1)^s\left(A^*_{pq}\frac{\partial}{\partial \xi} + B^*_{pq}\frac{\partial}{\partial \eta}\right)^s \frac{\partial^{k-s-1}}{\partial t^{k-s-1}}S_q. \tag{5}$$

*Proof.* We proof eqn. (5) by complete induction. For $k=0$ it is trivially fulfilled, so we start with $k=1$:

$$\frac{\partial}{\partial t}u_p = (-1)\left(A^*_{pq}\frac{\partial}{\partial \xi} + B^*_{pq}\frac{\partial}{\partial \eta}\right)u_q + S_p \tag{6}$$

Eqn. (6) is nothing else than eqn. (4) rewritten in a different form, so for $k=1$ formula (5) holds. If we now suppose that it holds for $k$, one can easily proof that from this assumption it will also hold for $k+1$. Deriving (5) with respect to time yields

$$\frac{\partial^{k+1}}{\partial t^{k+1}}u_p = (-1)^k\left(A^*_{pq}\frac{\partial}{\partial \xi} + B^*_{pq}\frac{\partial}{\partial \eta}\right)^k \frac{\partial}{\partial t}u_q + \sum_{s=0}^{k-1}(-1)^s\left(A^*_{pq}\frac{\partial}{\partial \xi} + B^*_{pq}\frac{\partial}{\partial \eta}\right)^s \frac{\partial^{k-s}}{\partial t^{k-s}}S_q, \tag{7}$$

which by using (6) becomes

$$\begin{aligned}\frac{\partial^{k+1}}{\partial t^{k+1}}u_p &= (-1)^k\left(A^*_{pq}\frac{\partial}{\partial\xi}+B^*_{pq}\frac{\partial}{\partial\eta}\right)^k\left((-1)\left(A^*_{qr}\frac{\partial}{\partial\xi}+B^*_{qr}\frac{\partial}{\partial\eta}\right)u_r+S_q\right)\\ &+ \sum_{s=0}^{k-1}(-1)^s\left(A^*_{pq}\frac{\partial}{\partial\xi}+B^*_{pq}\frac{\partial}{\partial\eta}\right)^s\frac{\partial^{k-s}}{\partial t^{k-s}}S_q\,.\end{aligned} \tag{8}$$

Rearranging terms yields

$$\begin{aligned}\frac{\partial^{k+1}}{\partial t^{k+1}}u_p &= (-1)^{k+1}\left(A^*_{pq}\frac{\partial}{\partial\xi}+B^*_{pq}\frac{\partial}{\partial\eta}\right)^{k+1}u_q+(-1)^k\left(A^*_{pq}\frac{\partial}{\partial\xi}+B^*_{pq}\frac{\partial}{\partial\eta}\right)^k S_q\\ &+ \sum_{s=0}^{k-1}(-1)^s\left(A^*_{pq}\frac{\partial}{\partial\xi}+B^*_{pq}\frac{\partial}{\partial\eta}\right)^s\frac{\partial^{k-s}}{\partial t^{k-s}}S_q,\end{aligned} \tag{9}$$

and finally

$$\frac{\partial^{k+1}}{\partial t^{k+1}}u_p = (-1)^{k+1}\left(A^*_{pq}\frac{\partial}{\partial\xi}+B^*_{pq}\frac{\partial}{\partial\eta}\right)^{k+1}u_q+\sum_{s=0}^{k}(-1)^s\left(A^*_{pq}\frac{\partial}{\partial\xi}+B^*_{pq}\frac{\partial}{\partial\eta}\right)^s\frac{\partial^{k-s}}{\partial t^{k-s}}S_q. \tag{10}$$

□

In order to be able to perform many computations in the reference element $T_E$, we represent the source-terms in a space-time basis over the space-time element $T_E\times[t^n;t^n+\Delta t]$. The basis is constructed via tensor product of the spatial basis functions $\Phi_m(\xi,\eta)$ used already in (3) and some new temporal basis functions $\Psi_l(t)$ for which we choose classical Legendre polynomials in the interval of one time step $[t^n;t^n+\Delta t]$:

$$S_p(\xi,\eta,t)=\hat{S}_{plm}\Psi_l(t)\Phi_m(\xi,\eta). \tag{11}$$

Given the source term $S_p(\xi,\eta,t)$ by some analytic function or from discrete measurement data, we first perform $L^2$ projection in order to compute the unknown coefficients $\hat{S}_{plm}$ in (11). In the following, $\langle .,.\rangle_{(\cdot)}$ denotes the inner product over the domain $(\cdot)$.

$$\left\langle S_p\left(\xi,\eta,t\right),\Psi_j\Phi_k\right\rangle_{T_E\times[t^n;t^n+\Delta t]}=\hat{S}_{plm}\left\langle\Psi_j\Phi_k,\Phi_m\Psi_l\right\rangle_{T_E\times[t^n;t^n+\Delta t]} \tag{12}$$

Since spatial and temporal integration are independent due to the tensor product formulation, we get

$$\left\langle S_p\left(\xi,\eta,t\right),\Psi_j\Phi_k\right\rangle_{T_E\times[t^n;t^n+\Delta t]}=\hat{S}_{plm}\left\langle\Psi_j,\Psi_l\right\rangle_{[t^n;t^n+\Delta t]}\left\langle\Phi_m,\Phi_k\right\rangle_{T_E}. \tag{13}$$

Due to the orthogonality of the basis functions, the appearing mass matrices are diagonal and can be trivially inverted.

As in (Käser & Dumbser 2005) we now develop the solution of (2) in a Taylor series in time up to order $N$,

$$u_p(\xi,\eta,t)=\sum_{k=0}^{N}\frac{t^k}{k!}\frac{\partial^k}{\partial t^k}u_p(\xi,\eta,0), \tag{14}$$

and replace time derivatives by space derivatives, using (3), (5) and (11):

$$\begin{aligned} u_p(\xi,\eta,t) &= \sum_{k=0}^{N} \frac{t^k}{k!} (-1)^k \left( A^*_{pq} \frac{\partial}{\partial \xi} + B^*_{pq} \frac{\partial}{\partial \eta} \right)^k \Phi_l \hat{u}_{ql}(0) \\ &+ \sum_{s=0}^{k-1} (-1)^s \left( A^*_{pq} \frac{\partial}{\partial \xi} + B^*_{pq} \frac{\partial}{\partial \eta} \right)^s \frac{\partial^{k-s-1}}{\partial t^{k-s-1}} \Psi_l(t) \Phi_m(\xi,\eta) \hat{S}_{qlm}. \end{aligned} \tag{15}$$

This approximation can now be projected onto each basis function in order to get an approximation of the evolution of the degrees of freedom during one time step from time level $n$ to time level $n+1$. We obtain

$$\int_0^{\Delta t} \hat{u}_{pl}(\tau) d\tau = I_{plqm}(\Delta t) \hat{u}_{qm}(0) + I^S_{plqom}(\Delta t) \hat{S}_{qom}, \tag{16}$$

with

$$I_{plqm}(\Delta t) = \frac{\left\langle \Phi_n, \sum\limits_{k=0}^{N} \frac{\Delta t^{(k+1)}}{(k+1)!} (-1)^k \left( A^*_{pq} \frac{\partial}{\partial \xi} + B^*_{pq} \frac{\partial}{\partial \eta} \right)^k \Phi_m(\xi) \right\rangle_{T_E}}{\langle \Phi_n, \Phi_l \rangle_{T_E}} \tag{17}$$

as in (Käser & Dumbser 2005) and an additional tensor taking into account the source term during time integration,

$$I^S_{plqom}(\Delta t) = \frac{\left\langle \Phi_n, \sum\limits_{k=0}^{N} \frac{\Delta t^{(k+1)}}{(k+1)!} \sum\limits_{s=0}^{k-1} (-1)^s \left( A^*_{pq} \frac{\partial}{\partial \xi} + B^*_{pq} \frac{\partial}{\partial \eta} \right)^s \Phi_m \frac{\partial^{k-s-1}}{\partial t^{k-s-1}} \Psi_o \right\rangle_{T_E}}{\langle \Phi_n, \Phi_l \rangle_{T_E}}. \tag{18}$$

To facilitate notation we skip the index $^{(m)}$ for the two tensors as given by (17) and (18) since they may vary from one element to another depending on the variation of the Jacobian matrices $A^*_{pq}$ and $B^*_{pq}$ .

With those definitions we finally obtain the fully discrete ADER-DG scheme, which differs from the one given in (Käser & Dumbser 2005) only with respect to the correction terms on the left hand side and the source terms on the right hand side of the equation.

$$\begin{aligned} & \left[ \left( \hat{u}^{(m)}_{pl} \right)^{n+1} - \left( \hat{u}^{(m)}_{pl} \right)^{n} \right] |J| \, M_{kl} \\ + \;& \tfrac{1}{2} \sum_{j=1}^{3} T^j_{pq} \left( A^{(m)}_{qr} + \left| A^{(m)}_{qr} \right| \right) (T^j_{rs})^{-1} \, |S_j| \, F^{j,0}_{kl} \cdot \left( I_{slmn}(\Delta t) \left( \hat{u}^{(m)}_{mn} \right)^n + I^S_{slmon}(\Delta t) \left( \hat{S}^{(m)}_{mon} \right)^n \right) \\ + \;& \tfrac{1}{2} \sum_{j=1}^{3} T^j_{pq} \left( A^{(m)}_{qr} - \left| A^{(m)}_{qr} \right| \right) (T^j_{rs})^{-1} \, |S_j| \, F^{j,i}_{kl} \cdot \left( I_{slmn}(\Delta t) \left( \hat{u}^{(m_j)}_{mn} \right)^n + I^S_{slmon}(\Delta t) \left( \hat{S}^{(m_j)}_{mon} \right)^n \right) \\ - \;& |J| \left( A^*_{pq} K^{\xi}_{kl} + B^*_{pq} K^{\eta}_{kl} \right) \cdot \left( I_{slmn}(\Delta t) \left( \hat{u}^{(m)}_{mn} \right)^n + I^S_{slmon}(\Delta t) \left( \hat{S}^{(m)}_{mon} \right)^n \right) \\ = \;& \int\limits_{t^n}^{t^n+\Delta t} \int\limits_{\mathcal{T}^{(m)}} \Phi_k \, S_p(x,y,t) \, dV \, dt = M_{kl} \cdot \int\limits_{0}^{\Delta t} \Psi_o(\tau) \, d\tau \cdot \hat{S}^{(m)}_{pol} . \end{aligned} \tag{19}$$

Note that $\tau = t - t^n$. On rectangular elements, the scheme takes the same form except that one has to consider the contribution of four edges instead of three in the case of triangles. For the efficient evaluation of expressions (17) and (18) the same algorithm as presented by Käser and Dumbser (2005) can be used.

### 3.2 Point Sources

In the previous subsection we described the discretization of source terms that are continuous in space and time. However, many geophysical applications as well as classical test cases with analytical solutions, such as e.g. Lamb's problem or Garvin's problem, require point sources that are characterized by a Dirac Delta distribution in space and a so-called source time function $S_p^T(t)$. Within the ADER-DG framework, it is straightforward to include such point sources at *arbitrary* positions in the computational domain. It is *not* necessary that the Delta distributions coincide with a grid point since the arising integrals can always be evaluated analytically using the properties of the Delta distribution. The source terms considered in this subsection thus have the form

$$S_p(x, y, t) = S_p^T(t) \cdot \delta(\vec{x} - \vec{x}_s), \tag{20}$$

where $\delta(\vec{x})$ denotes the usual Dirac Delta distribution with its well-known properties. Since the source term is given in space by the Delta distribution, we only have to project the time-dependent part, i.e. the source time function $S_p^T(t)$, onto some temporal basis functions similar to subsection 3.1 by simply requiring that

$$\left\langle \Psi_j, S_p^T(t) \right\rangle_{[t^n;t^n+\Delta t]} = \left\langle \Psi_j, \hat{S}_{pl}\Psi_l \right\rangle_{[t^n;t^n+\Delta t]}, \tag{21}$$

which leads to the following discrete representation of the point source:

$$S_p(x, y, t) = \hat{S}_{pl}\Psi_l(t) \cdot \delta(\vec{x} - \vec{x}_s). \tag{22}$$

Similar to eqn. (16) we obtain the following expression that can be directly inserted on the left hand side of eqn. (19),

$$\int_0^{\Delta t} \hat{u}_{pl}(\tau)d\tau = I_{plqm}(\Delta t)\hat{u}_{qm}(0) + I^S_{plqm}(\Delta t)\hat{S}_{qm}, \tag{23}$$

with $I_{plqm}(\Delta t)$ still given by eqn. (17) and a correction term $I^S_{plqm}(\Delta t)$ due to the point source given by

$$I^S_{plqm}(\Delta t) = \frac{\sum\limits_{k=0}^{N} \frac{\Delta t^{(k+1)}}{(k+1)!} \sum\limits_{s=0}^{k-1} \left( A^*_{pq}\frac{\partial}{\partial \xi} + B^*_{pq}\frac{\partial}{\partial \eta} \right)^s \Phi_n\left(\vec{\xi}_s\right) \cdot \frac{\partial^{k-s-1}}{\partial t^{k-s-1}}\Psi_m}{|J| \left\langle \Phi_n, \Phi_l \right\rangle_{T_E}}. \tag{24}$$

if the point source is located inside the corresponding element, i.e. $\vec{x}_s \in \mathcal{T}^{(m)}$, or zero elsewhere. Note that $\vec{\xi}_s$ is the location of the point source in the reference element. Eqn. (24) follows directly from (18) using the properties of the Delta distribution and its derivatives. The right hand side of eqn. (19) reduces to zero except of those elements that contain the point sources, where it then becomes

$$\int_{t^n}^{t^n+\Delta t} \int_{\mathcal{T}^{(m)}} \Phi_k \, S_p(x,y,t) \, dV \, dt = \Phi_k \left( \vec{x}_s \right) \cdot \int_{t^n}^{t^n+\Delta t} S_p^T(t) dt. \tag{25}$$

Since the test functions are evaluated exactly at the source position $\vec{x}_s$, the point sources may be located at *any* point inside the computational domain. If the point $\vec{x}_s$ coincides with a grid point or cell edge, only one of the adjacent elements is allowed to contain the source. The choice, however, is arbitrary.

## 4 CONVERGENCE STUDY

In order to validate the discretization of the source terms we study the convergence rates on the example of a fourth and sixth order ADER-DG scheme on a regular triangular grid such as presented in (Käser & Dumbser 2005). The source term is constructed such that the solution of the elastic wave equations with source terms (2) becomes the space-time periodic function

$$u_p(x,y,t) = U_p^0 \cdot \sin\left(\frac{2\pi}{\lambda_p^x} x\right) \cdot \sin\left(\frac{2\pi}{\lambda_p^y} y\right) \cdot \sin\left(\frac{2\pi}{T_p} t\right). \tag{26}$$

For the amplitudes, spatial wave lengths and time periods of the five variables we choose in our particular example the vectors

$$U_p^0 = \begin{pmatrix} 1 & 2 & 3 & 4 & 5 \end{pmatrix}^T, \tag{27}$$

$$\lambda_p^x = \lambda_p^y = \begin{pmatrix} 33\frac{1}{3} & 50 & 100 & 50 & 33\frac{1}{3} \end{pmatrix}^T, \tag{28}$$

$$T_p = \begin{pmatrix} 33\frac{1}{3} & 50 & 100 & 10 & 5 \end{pmatrix}^T. \tag{29}$$

The spatial and temporal derivatives of the imposed solution (26) can be computed as

$$\frac{\partial}{\partial x} u_p(x,y,t) = U_p^0 \cdot \frac{2\pi}{\lambda_p^x} \cdot \cos\left(\frac{2\pi}{\lambda_p^x} x\right) \cdot \sin\left(\frac{2\pi}{\lambda_p^y} y\right) \cdot \sin\left(\frac{2\pi}{T_p} t\right), \tag{30}$$

$$\frac{\partial}{\partial y} u_p(x,y,t) = U_p^0 \cdot \frac{2\pi}{\lambda_p^y} \cdot \sin\left(\frac{2\pi}{\lambda_p^x} x\right) \cdot \cos\left(\frac{2\pi}{\lambda_p^y} y\right) \cdot \sin\left(\frac{2\pi}{T_p} t\right), \tag{31}$$

$$\frac{\partial}{\partial t} u_p(x,y,t) = U_p^0 \cdot \frac{2\pi}{T_p} \cdot \sin\left(\frac{2\pi}{\lambda_p^x} x\right) \cdot \sin\left(\frac{2\pi}{\lambda_p^y} y\right) \cdot \cos\left(\frac{2\pi}{T_p} t\right), \tag{32}$$

and thus the source terms are directly given by the governing equations (2) themselves. The two-dimensional elastic wave equations in (1) are solved on a square shaped domain $\Omega = [-50, 50] \times [-50, 50] \in \mathbb{R}^2$ with four periodic boundary conditions up to the final time $t = 100$. This means that the waves in the five variables oscillate for 3, 2, 1, 10 and 20 periods, respectively. Especially due to the rather high temporal frequencies of the last two variables, we expect the accuracy of the time discretization to be of great importance. We note that the initial condition is zero everywhere which is hence also the exact solution after $t = 100$. The CFL number is set in all computations to $70\%$ of the stability limit $\frac{1}{2N+1}$ of Runge-Kutta DG schemes.

Two different numerical experiments are performed. First, the scheme is implemented as given by equation (19). Second, we neglect the influence of the source terms in the Cauchy-Kovalewski procedure by simply setting $I^S_{slmon}$ to zero in (19). This would mean that the source term is only considered on the right hand side but not inside the wave propagation operator on the left hand side. For the regular mesh that we are using for this test case, the refinement is simply controlled by changing the number $N_G$ of grid cells in each dimension.

In Table 1 the errors in $L^\infty$ and $L^2$ norm of the vertical velocity $v$ are given as a function of $N_G$. The corresponding numerical convergence orders $\mathcal{O}_{L^\infty}$ and $\mathcal{O}_{L^2}$ are determined by two successively refined meshes. Furthermore, we present the total number $N_d$ of degrees of freedom.

We clearly see from table 1 that the designed fourth and sixth order of accuracy has been reached, respectively, in the case where we correctly include the source term in the Cauchy-Kovalewski procedure. However, if we neglect it, only second order of accuracy is retrieved globally. This result clearly emphasizes the importance of highly accurate time-discretization for time-dependent problems.

## 5 NUMERICAL EXAMPLES WITH ANALYTICAL SOLUTIONS

Here we present two well-known test cases of computational seismology in order to demonstrate the performance of the proposed ADER-DG scheme considering two different kinds of point sources, namely a vertical force and an explosive source, respectively, in a homogeneous elastic half-space with a free surface. For both test cases there are analytical reference solutions available. In addition to the validation of the discretization of the source terms, the implementation of the correct free surface boundary conditions is confirmed.

### 5.1 Lamb's Problem

A classical test case to validate the implementation of free surface boundary conditions and point sources is Lamb's Problem (Lamb 1904), consisting in a vertical (with respect to the surface) point force acting *on* the free surface. The solution of Lamb's Problem for a plane surface can be computed

**Table 1.** Convergence rates of $v$ for 4th and 6th order ADER-DG schemes with (top) and without (bottom) including the source terms in the Cauchy-Kovalewski procedure.

| ADER-DG $\mathcal{O}4$ | | | | | |
|---|---|---|---|---|---|
| $N_G$ | $L^\infty$ | $\mathcal{O}_{L^\infty}$ | $L^2$ | $\mathcal{O}_{L^2}$ | $N_d$ |
| 10 | $3.713 \cdot 10^{-2}$ | – | $1.243 \cdot 10^{-0}$ | – | 4000 |
| 20 | $6.821 \cdot 10^{-4}$ | 5.8 | $1.942 \cdot 10^{-2}$ | 6.0 | 16000 |
| 40 | $1.891 \cdot 10^{-5}$ | 5.2 | $4.113 \cdot 10^{-4}$ | 5.6 | 64000 |
| 50 | $5.801 \cdot 10^{-6}$ | 5.3 | $1.294 \cdot 10^{-4}$ | 5.2 | 100000 |
| 10 | $3.363 \cdot 10^{-2}$ | – | $1.190 \cdot 10^{-0}$ | – | 4000 |
| 20 | $1.000 \cdot 10^{-3}$ | 5.1 | $2.560 \cdot 10^{-2}$ | 5.5 | 16000 |
| 40 | $1.004 \cdot 10^{-4}$ | 3.3 | $3.569 \cdot 10^{-3}$ | 2.8 | 64000 |
| 50 | $5.844 \cdot 10^{-5}$ | 2.4 | $2.292 \cdot 10^{-3}$ | 2.0 | 100000 |

| ADER-DG $\mathcal{O}6$ | | | | | |
|---|---|---|---|---|---|
| $N_G$ | $L^\infty$ | $\mathcal{O}_{L^\infty}$ | $L^2$ | $\mathcal{O}_{L^2}$ | $N_d$ |
| 5 | $7.556 \cdot 10^{-3}$ | – | $2.217 \cdot 10^{-1}$ | – | 2100 |
| 10 | $2.376 \cdot 10^{-4}$ | 5.0 | $7.600 \cdot 10^{-3}$ | 4.9 | 8400 |
| 20 | $7.782 \cdot 10^{-7}$ | 8.3 | $1.720 \cdot 10^{-5}$ | 8.8 | 33600 |
| 30 | $4.752 \cdot 10^{-8}$ | 6.9 | $9.750 \cdot 10^{-7}$ | 7.1 | 75600 |
| 5 | $8.571 \cdot 10^{-3}$ | – | $2.865 \cdot 10^{-1}$ | – | 2100 |
| 10 | $1.129 \cdot 10^{-3}$ | 2.9 | $4.158 \cdot 10^{-2}$ | 2.8 | 8400 |
| 20 | $2.290 \cdot 10^{-4}$ | 2.3 | $8.603 \cdot 10^{-3}$ | 2.3 | 33600 |
| 30 | $7.400 \cdot 10^{-5}$ | 2.8 | $3.084 \cdot 10^{-3}$ | 2.5 | 75600 |

analytically and can hence be used for comparison with numerical results. In this paper we use the FORTRAN code `EX2DDIR` of Berg and If⋆ to compute the exact solution of the seismic 2-D response from a vertical directional point source in an elastic half space with a free surface. The code `EX2DDIR` is based on the Cagniard-de Hoop technique (de Hoop 1960) and allows the use of an arbitrary source time function for displacements or velocities. Considering the accuracy of a numerical method and the correct treatment of sources and free boundary conditions Lamb's Problem poses a challenging test case in particular for the non-dispersive Rayleigh waves propagating along a plane free surface of an homogeneous half space.

⋆Laboratory of applied mathematical physics, Technical University of Denmark, Lyngby.

The setup of the physical problem is chosen as in the paper of Komatitsch and Vilotte (1998), who solved this problem using the Spectral Element method, see e.g. (Komatitsch & Tromp 1999; Komatitsch & Tromp 2002).

We use a homogeneous elastic medium with a P-wave velocity of $c_p = 3200\,m\,s^{-1}$, an S-wave velocity of $c_s = 1847.5\,m\,s^{-1}$ and a mass density of $\rho = 2200\,kg\,m^{-3}$. The numerical model with origin $(0,0)$ at the left bottom corner is $4000\,m$ wide and has a height of $2000\,m$ on the left boundary. The tilt angle of the free surface is $\phi = 10^\circ$. The directional point source, acting as a force perpendicular to this tilted surface, is located at the free surface at $\vec{x}_s = (1720.00,\ 2303.28)^T$. The two receivers are located at $(2694.96,\ 2475.18)$ and $(3400.08,\ 2599.52)$ such that their distances from the source along the surface are $990\,m$ and $1706\,m$, respectively. On the left, right and bottom boundaries of the model we use then open boundary conditions as described in (Käser & Dumbser 2005). We use a triangular mesh such that the left and right boundaries of the model are discretised by 30 triangle edges and the bottom and top boundaries by 50 triangles, similar to Komatitsch and Vilotte (1998). The resulting mesh is displayed in Fig. 1 (top) and consists of $3416$ triangles. In order to avoid undesired effects of possibly reflected wave energy at the right model boundary, we extended the mesh up to a width of $4700\,m$ for the numerical computations. The source time function that specifies the temporal variation of the point source is a Ricker wavelet given by

$$S^T(t) = a_1\left(0.5 + a_2(t - t_D)^2\right)e^{a_2(t-t_D)^2}, \tag{33}$$

where $t_D = 0.08\,s$ is the source delay time and $a_1 = -2000\,kg\,m^{-2}\,s^{-2}$ and $a_2 = -(\pi f_c)^2$ are constants determining the amplitude and frequency of the Ricker wavelet of central frequency $f_c = 14.5$ Hz.

The final resulting source vector $S_p(x,y,t)$ acting on the governing PDE (1) or (2), respectively, taking into account also the tilt angle $\phi$ is

$$S_p(x,y,t) = \begin{pmatrix} 0 & 0 & 0 & -\sin(\phi) & \cos(\phi) \end{pmatrix}^T \cdot \frac{S^T(t)}{\rho} \cdot \delta\left(\vec{x} - \vec{x}_s\right). \tag{34}$$

The wave propagation is simulated until time $T_{end} = 1.3\,s$ when all waves have already passed the two receivers. For the results shown in this paper, a tenth order ADER-DG $\mathcal{O}10$ scheme with a Courant number of CFL $= 0.5$ is used. In order to reach the final simulation time $T_{end}$ we need 5915 time steps. We then perform the same simulation on a refined mesh, where the mesh spacing is gradually decreasing towards the free surface, see Fig. 1(bottom). This problem-adapted mesh helps to resolve surface effects, such as the Rayleigh waves, with higher accuracy and requires 8836 time steps to reach $T_{end}$. In Fig. 1 we present the snapshots of the vertical velocity component $v$ of the seismic wave field at $t = 0.6s$ on a regular (top) and refined (bottom) triangular mesh. We remark, that the total number of triangles used in both simulations is the same. Visually, there is a perfect match between both numerical solutions. In Fig. 2 we present the unscaled seismograms obtained from our numerical simulations, as recorded by receiver 1 and 2, respectively, together with the analytical solution provided by `EX2DDIR`. The analytical and numerical solutions match extremely well, such that the lines basically are not distinguishable on this scale. Therefore, the residuals are also plotted and are amplified by a factor of 10 in order to make differences more visible. The maximum relative error on the regular mesh remains always less than 1%, however, it is considerably smaller on the surface-refined mesh where it is about 0.3%. We conclude from this example that correctly including the source terms in the Cauchy-Kovalewski procedure is also beneficial with respect to accuracy in the context of point sources. In particular, for point sources the additional computational effort is very small, as the Cauchy-Kovalewski procedure with source terms appears only in the triangle, where the point sources is located. In addition, the accurate solution of Lamb's problem with the ADER-DG method confirms, that the implementation of free surface boundary conditions as suggested in (Käser & Dumbser 2005) leads to the correct physical behaviour of elastic surface waves.

### 5.2 Garvin's Problem

Another classical test case to validate the implementations of free surface boundary conditions and point sources is Garvin's Problem (Garvin 1956), which consists in an explosive point source located *below*, but close to the surface. As for Lamb's problem the solution of Garvin's Problem for a plane surface can be computed analytically. In this paper we use the FORTRAN code `EX2DVAEL` of Berg and If to compute the exact solution of the seismic 2-D response from an explosive point source in an elastic half space with a free surface. Similar to Lamb's problem, the computation of this reference solution is based on the Cagniard-de Hoop technique (de Hoop 1960) and allows the use of an arbitrary source time function for displacements or velocities.

The setup of the physical problem as well as all the numerical parameters remain essentially the same as for Lamb's problem presented in the previous subsection 5.1. Especially the two receivers remain at the same locations. However, with respect to the source location in Lamb's problem, the source position is now located $100$m *below* the free surface (in normal direction to the free surface), such that $\vec{x}_s = (1737.36,\ 2204.80)^T$. The source time function that specifies the temporal variation of the point source is again given by (33) with the parameters $t_D = 0.08\,s$, $a_1 = 10^9\,N\,m^{-2}\,s^{-1}$ and $a_2 = -(\pi f_c)^2$. The central frequency $f_c = 14.5$ Hz remains unchanged. The finally resulting source vector $S_p(x,y,t)$ acting as an explosive source on the governing PDE (1) or (2), respectively, is then given by

$$S_p(x,y,t) = \begin{pmatrix} 1 & 1 & 0 & 0 & 0 \end{pmatrix}^T \cdot S^T(t) \cdot \delta\left(\vec{x} - \vec{x}_s\right). \tag{35}$$

The wave propagation is again simulated with a tenth order ADER-DG $\mathcal{O}10$ scheme at a Courant number of CFL $= 0.5$ until time $T_{end} = 1.3\,s$ on the same meshes as already used for Lamb's problem. In Fig. 3 we present a snapshot of the vertical velocity component $v$ of the seismic wave field at $t = 0.5s$ on the regular triangular mesh (top) and the problem-adapted, refined mesh (bottom). The two numerical solutions in Fig. 3 again match perfectly. In Fig. 4 we present the unscaled seismograms obtained from our numerical simulations at receiver 1 and 2, respectively, as well as the analytical solution. The residuals are also plotted and are amplified by a factor of 10 in order to make the visible. The maximal relative error again is of the order of 1%.

Having a closer look at the seismograms we see the effect of the mesh refinement. Considering the arrival of the direct wave, mesh refinement decreases the residuals similar to the seismograms for Lamb's problem in Fig. 2. However, if we look at the arrival of the generated surface wave for Garvin's problem, the residuals seem to slightly increase with mesh refinement. This effect is not completely clear, but might be due to the fact that during the simulation we are trying to approximate the spatial Dirac Delta distribution of the source term by a polynomial of degree 9. Due the mesh refinement, the position of the Dirac Delta impulse inside the enclosing triangle will change with respect to the reference triangle. Therefore, it might be possible, that the polynomial approximation becomes worse depending on the position of the Dirac Delta inside the triangle. However, this does not seem to affect the accuracy of the direct wave, but only the accuracy of the surface wave. We mention that this effect is relatively small, considering that we amplify the residuals by a factor of 10.

## 6 DISCUSSION AND CONCLUSIONS

We extended the ADER-DG method for the solution of linear hyperbolic systems on unstructured triangular meshes, as described e.g. in (Dumbser 2005; Dumbser & Munz 2005; Käser & Dumbser 2005) for the homogeneous case, to handle space-time dependent source terms.

We have shown numerical convergence studies with smooth source terms in space and time for fourth and sixth order ADER-DG schemes on regular triangular meshes confirming that uniformly very high accuracy in space and time are maintained when the source term is correctly included in the underlying Cauchy-Kovalewski procedure. Furthermore, we demonstrated that the global order of accuracy cannot be maintained if the source term is not correctly included in the time discretization, which clearly points out the necessity of treating smooth source terms according to the desired order of the numerical scheme.

Special attention has also been paid to the treatment of point sources, which can be located at *any* position inside the computational domain, i.e. inside a triangular cell. To this end we are using the properties of the Dirac Delta distribution in combination with evaluating the test functions at the source positions.

Furthermore the demonstrated test cases of Lamb's and Garvin's problem confirm that the free surface boundary condition, as introduced in previous work (Käser & Dumbser 2005), is treated correctly. Therefore, we claim that the newly proposed ADER-DG method can very well serve as an attractive alternative to the currently very popular Spectral Element method in particular in the field of computational seismology.

## ACKNOWLEDGMENTS

The authors thank the DFG (Deutsche Forschungsgemeinschaft), as the work was supported through the *Emmy Noether-Programm* (KA 2281/1-1) and the DFG-CNRS research group FOR 508, *Noise Generation in Turbulent Flows*. The helpful comments and hints of G. Seriani, D. Komatitsch, and Enrique Mercerat, in particular for obtaining the analytic reference solutions for Lamb's and Garvin's problem are highly appreciated.

## REFERENCES

Aki, K. & Richards, P.G., 2002. *Quantitative Seismology*, University Science Books.

Bedford, A. & Drumheller, D.S., 1994. *Elastic Wave Propagation*, Wiley.

de Hoop, A.T., 1960. A modification of Cagniard's method for solving seismic pulse problems, *Appl. Sci. Res.*, **B8**, 349-356.

Dumbser, M., 2005. Arbitrary High Order Schemes for the Solution of Hyperbolic Conservation Laws in Complex Domains, *PhD Thesis*, Universität Stuttgart, Institut für Aerodynamik und Gasdynamik.

Dumbser, M. & Munz, C.D., 2005. Arbitrary High Order Discontinuous Galerkin Schemes , in *Numerical Methods for Hyperbolic and Kinetic Problems*, eds. Cordier, S., Goudon, T., Gutnic, M. & Sonnendrucker, E., IRMA series in mathematics and theoretical physics, EMS Publishing House, 295–333.

Garvin, W., 1956. Exact Transient Solution of the Buried Line Source Problem, *Proceedings of the Royal Society of London. Series A*, **234**, 528-541.

Käser, M. & Dumbser, M., 2005. An Arbitrary High Order Discontinuous Galerkin Method for Elastic Waves on Unstructured Meshes I: The Two-Dimensional Isotropic Case, submitted to *Geophys. Prosp.*.

Käser, M. & Iske, A., 2005. ADER Schemes on Adaptive Triangular Meshes for Scalar Conservation Laws, *J. Comput. Phys.*,**205**,486-508.

Komatitsch, D. & Tromp, J., 1999. Introduction to the spectral-element method for 3-D seismic wave propagation, *Geophys. J. Int.*, **139**, 806-822.

Komatitsch, D. & Tromp, J., 2002. Spectral-element simulations of global seismic wave propagation - I. Validation, *Geophys. J. Int.*, **149**, 390-412.

Komatitsch, D. & Vilotte, J.P., 1998. The spectral-element method: an efficient tool to simulate the seismic response of 2D and 3D geological structures, *Bull. Seism. Soc. Am.*, **88**, 368-392.

Lamb, H., 1904. On the propagation of tremors over the surface of an elastic solid, *Phil. Trans. R. Soc. London. Ser. A*, **203**, 1-42.

LeVeque, R.L., 2002. *Finite Volume Methods for Hyperbolic Problems*, Cambridge University Press, Cambridge.

Schwartzkopff, T., Dumbser, M. & Munz, C.D., 2004. Fast high order ADER schemes for linear hyperbolic equations, *J. Comput. Phys.*, **197**, 532-539.

Titarev, V.A. & Toro, E.F., 2002. ADER: Arbitrary high order Godunov approach, *J. Sci. Comput.*, **17**, 609-618.

Toro, E.F., Millington, A.C. & Nejad, L.A., 2001. Towards very high order Godunov schemes, in *Godunov methods; Theory and applications*, Kluwer Academic Plenum Publishers, Oxford, 907-940.

Toro, E.F. & Titarev, V.A. 2002. Solution of the generalized Riemann problem for advection-reaction equations, *Proc. Roy. Soc. London*, 271-281.

**LIST OF FIGURES**

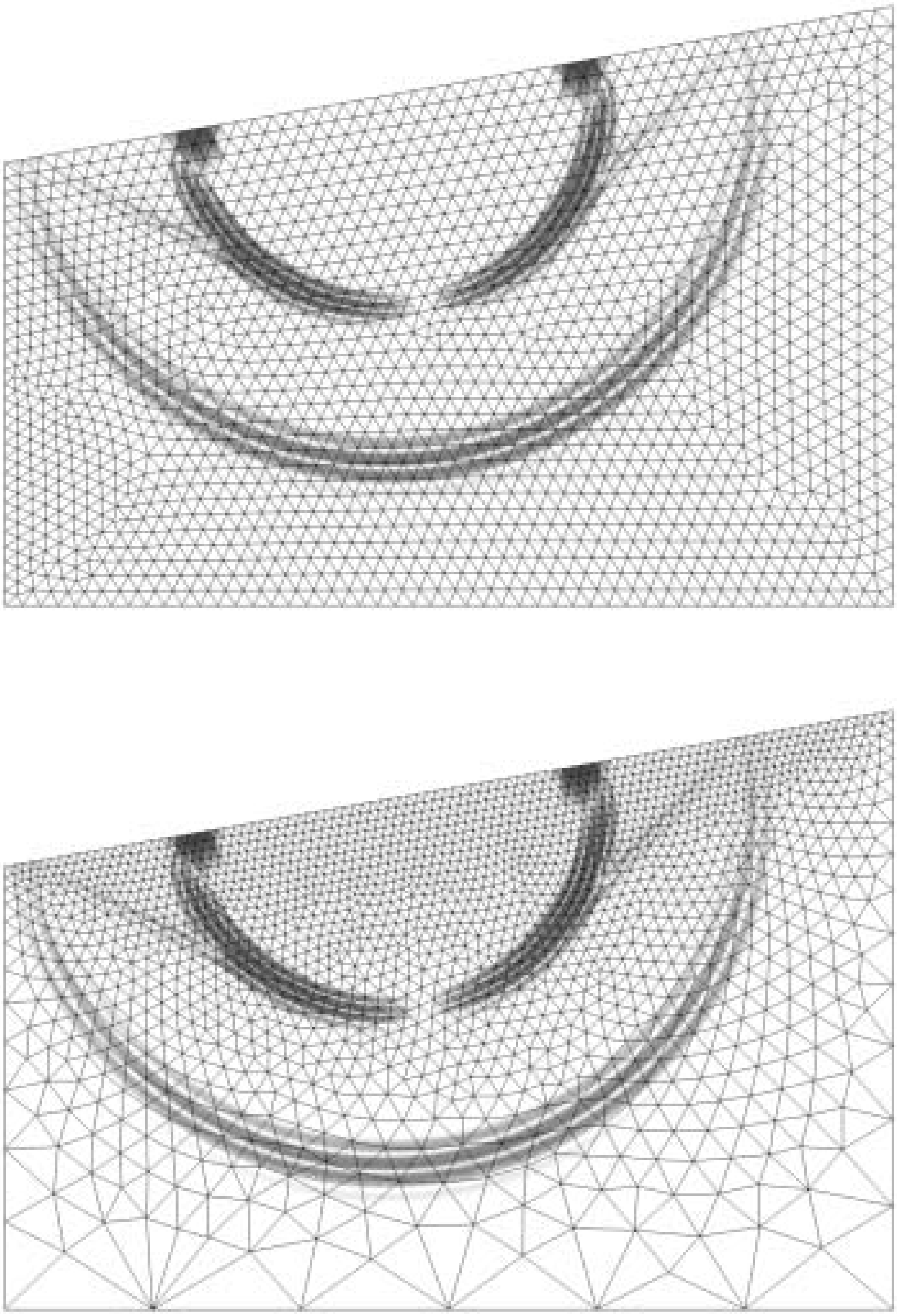

**Figure 1.** Vertical velocity $v$ at $t = 0.6s$ for Lamb's problem.
ADER-DG $\mathcal{O}10$ scheme on a regular (top) and refined (bottom) triangular mesh.

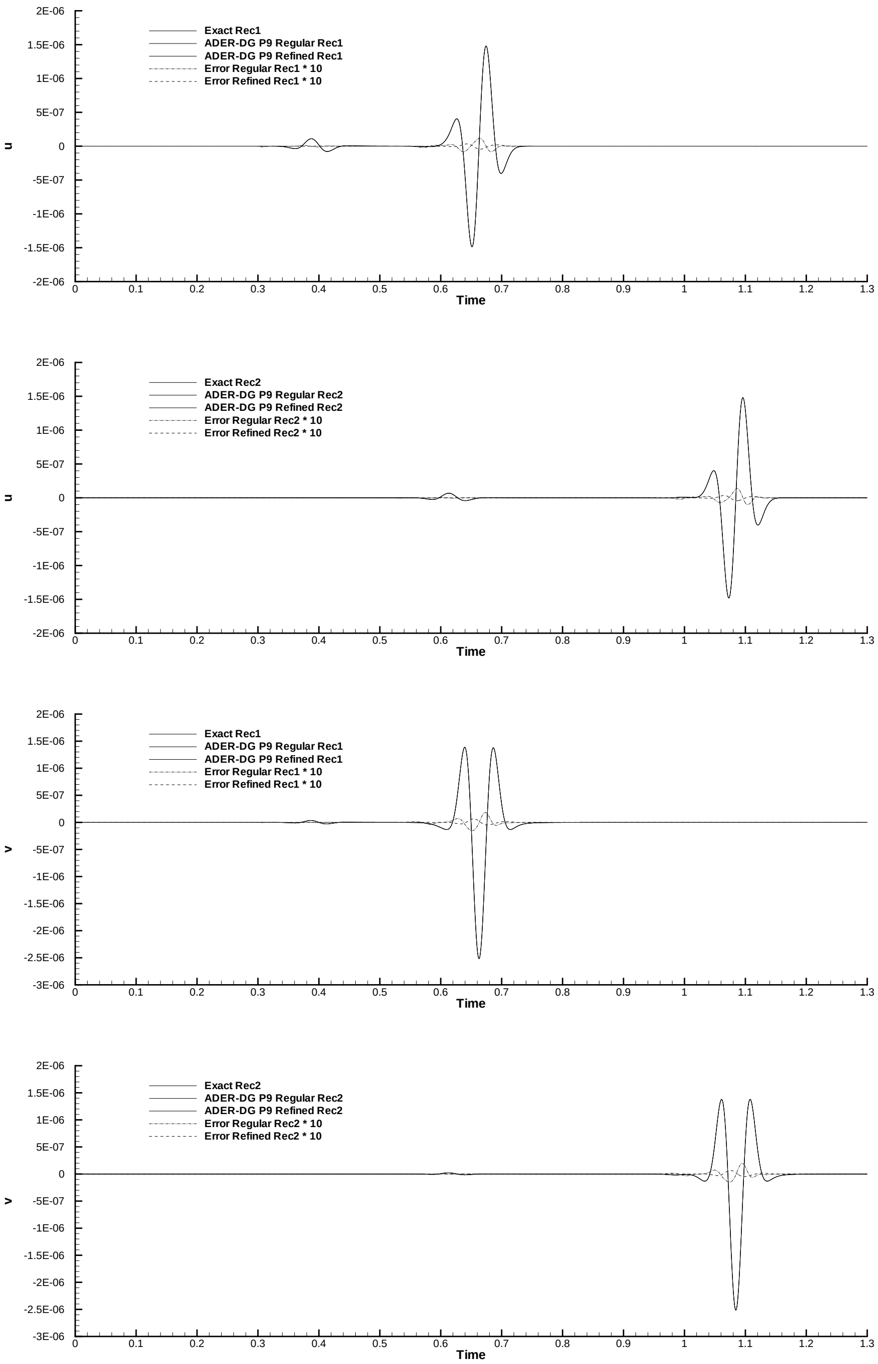


**Figure 2.** Seismograms of the normal and tangential velocity components w.r.t. the surface at the two receivers 1 and 2 for Lamb's problem.

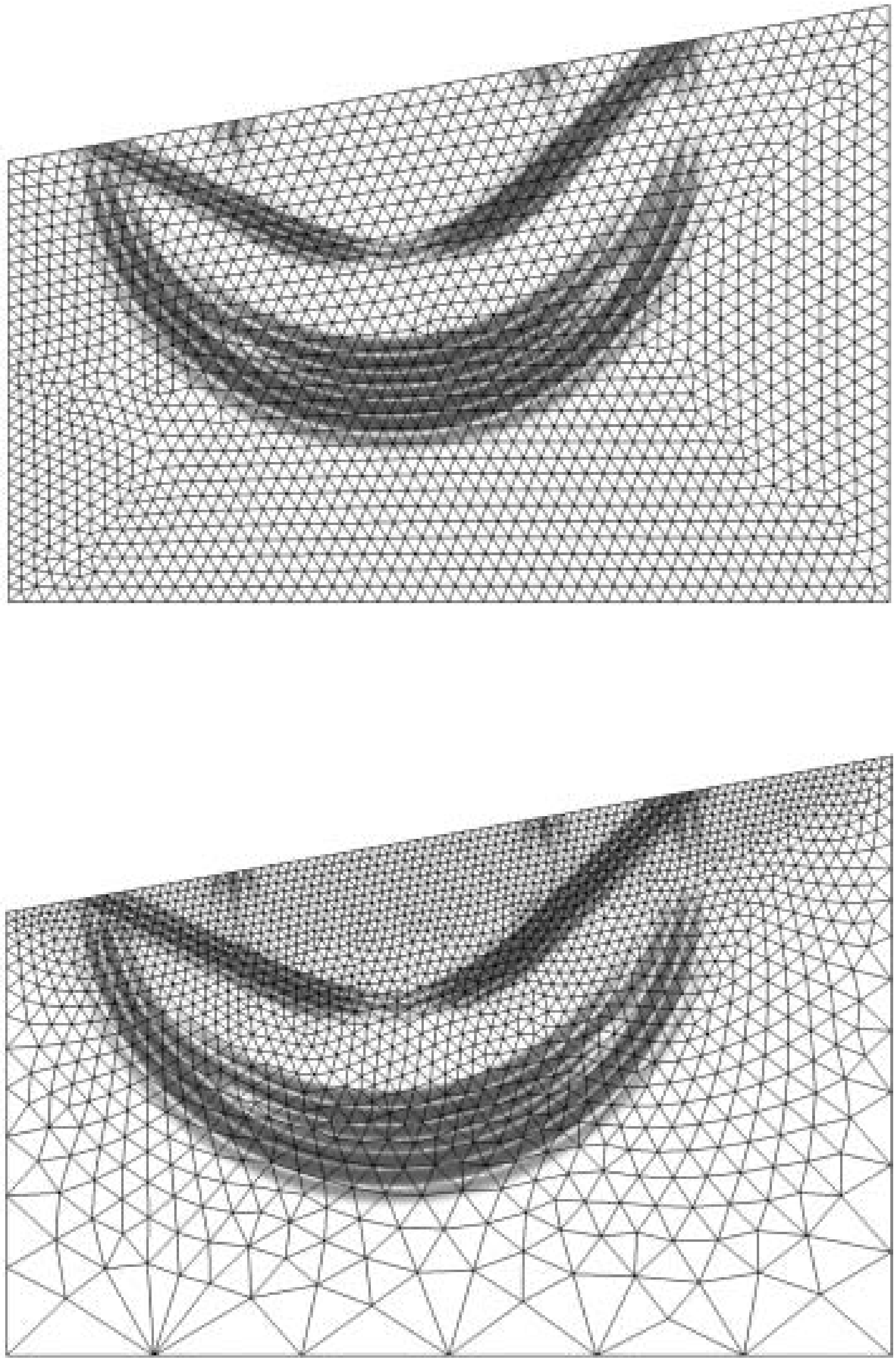

**Figure 3.** Vertical velocity $v$ at $t = 0.6s$ for Garvin's problem.

ADER-DG $\mathcal{O}10$ scheme on a regular (top) and refined (bottom) triangular mesh.

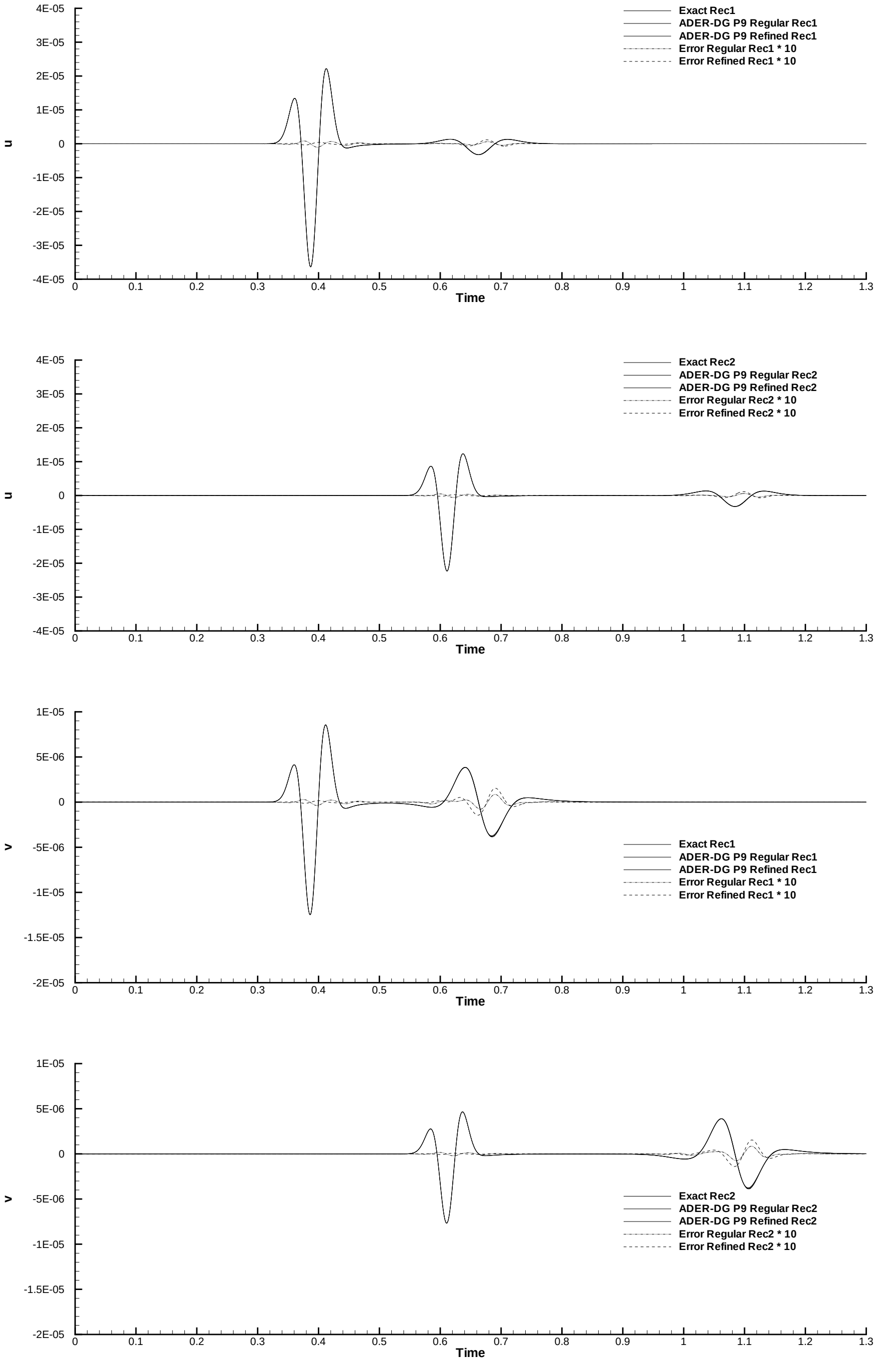


**Figure 4.** Seismograms of the normal and tangential velocity components w.r.t. the surface at the two receivers 1 and 2 for Garvin's Problem.